Topological acoustic polaritons: robust sound manipulation at the subwavelength scale

New Journal of Physics
The open access journal at the forefront of physics

Deutsche Physikalische Gesellschaft DPG
IOP Institute of Physics

Published in partnership with: Deutsche Physikalische Gesellschaft and the Institute of Physics

OPEN ACCESS

RECEIVED
30 November 2016

REVISED
24 February 2017

ACCEPTED FOR PUBLICATION
15 March 2017

PUBLISHED
20 July 2017

PAPER

Topological acoustic polaritons: robust sound manipulation at the subwavelength scale

Simon Yves[1], **Romain Fleury**[1,2], **Fabrice Lemoult**[1], **Mathias Fink**[1] **and Geoffroy Lerosey**[1]

[1] Institut Langevin, CNRS UMR 7587, ESPCI Paris, PSL Research University, 1 rue Jussieu, Paris F-75005, France
[2] Laboratory of Wave Engineering, Institute of Electrical Engineering, EPFL, 1015 Lausanne, Switzerland

E-mail: romain.fleury@epfl.ch

Keywords: acoustic metamaterials, topological insulators, polaritons, quantum spin Hall effect

Supplementary material for this article is available online

Abstract

Topological insulators, a hallmark of condensed matter physics, have recently reached the classical realm of acoustic waves. A remarkable property of time-reversal invariant topological insulators is the presence of unidirectional spin-polarized propagation along their edges, a property that could lead to a wealth of new opportunities in the ability to guide and manipulate sound. Here, we demonstrate and study the possibility to induce topologically non-trivial acoustic states at the deep subwavelength scale, in a structured two-dimensional metamaterial composed of Helmholtz resonators. Radically different from previous designs based on non-resonant sonic crystals, our proposal enables robust sound manipulation on a surface along predefined, subwavelength pathways of arbitrary shapes.

1. Introduction

Exciting discoveries in solid state physics have recently uncovered the intriguing properties of condensed matter with topological electronic properties [1–10]. Topological insulators, in particular, do not support electronic transport in their bulk, but allow for topologically protected unidirectional conduction on their edges [9, 10]. The presence of robust edge states in these systems arises from the topologically nontrivial nature of their band structure, which cannot change across space without closing the band gap, implying the existence of conductive states at interfaces between domains of distinct topology, with topological resilience to structural defects, local disorder and other continuous perturbations. This finding has lately spawned a quest to obtain similar properties for classical [11–56] and bosonic [57, 58] systems, including electromagnetic [11–37], mechanical [38–46] or acoustic [47–56] systems. Indeed, topological physics promises many new opportunities in the context of signal transport, including backscattering immune one-way propagation [14], an increased ability to tame the path of the signal in complex environments [47, 51], and stronger robustness to perturbations, fabrication defects and disorder [22].

Nevertheless, the physics of light, sound, and mechanical wave propagation is fundamentally different than the one of electrons, and finding classical analogs to electronic topological insulators imply solving a certain number of challenges. Chern topological insulators [1–3, 11–14, 16, 43, 44, 47, 48, 50, 51, 53, 55], on one hand, require violating time-reversal (TR) symmetry, which implies to largely break reciprocity of wave propagation [59], a difficult task in linear photonic [60] or acoustic [61–64] systems. In addition, this usually involves the use of a time-odd external bias, such as a magnetic field, often leading to designs that require some form of external energy input, and an arguably challenging implementation. On the other hand, TR invariant topological insulators [4–10, 15, 17–42, 45, 46, 49, 52, 54, 56] are generally passive, but rely on the presence of Kramers partners carried by the spin degree of freedom, absent in bosonic systems. Nevertheless, by employing adequate pseudo-spin engineering tricks, exploiting electromagnetic duality [17, 24, 29, 35], judiciously coupled lattices [45, 56], or other forms of internal symmetries [31, 32, 54], this type of topological insulators has also been demonstrated for electromagnetic, mechanical and acoustic waves.

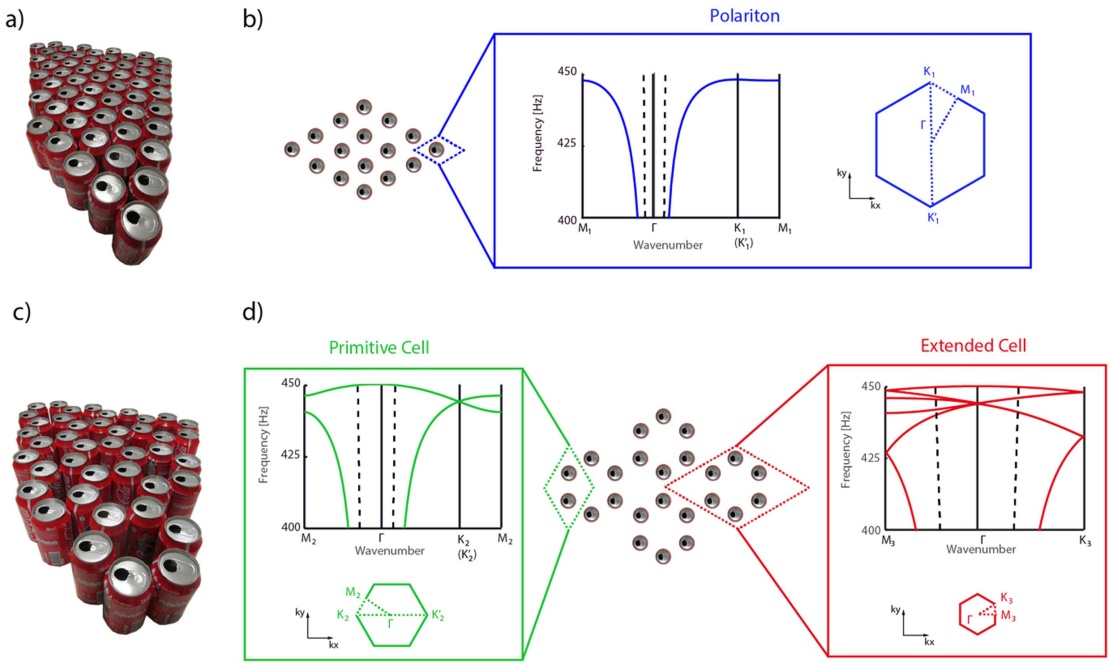

Figure 1. Examples of two-dimensional, subwavelength arrays of Helmholtz resonators that support spoof surface acoustic polaritons. A triangular lattice (a) possesses one resonator per unit cell (panel (b), dashed box), leading to a single polaritonic band below the individual resonance frequency of the resonators (450 Hz). By changing the subwavelength structure of the metamaterial, it is possible to engineer the band structure at will. Panel (c) considers the case of a honeycomb lattice, which features Dirac cone at K2 and K2′ (primitive cell description, green box). In the extended cell description (red box), the time-reversed Dirac cones at K2 and K2′ fold into the Γ point, creating four-fold degeneracy at the center of the Brillouin zone. These degenerate time-reversed polaritons emulate electronic Kramers pairs, providing an ideal starting point to induce nontrivial topology.

In audible acoustics, particularly, one of the principal challenge is the large scale of the wavelength involved, that typically necessitates bulky structures in order to control sound propagation. For instance, the recent experimental demonstration of a TR invariant acoustic topological insulator was based on a sonic crystal with 6-fold rotational symmetry [54]. Such sonic crystals are typically limited by their granularity: being based on Bragg interferences, they can only guide sound on scales comparable to the wavelength. On the other hand, subwavelength wave control can be achieved in resonant metamaterials, which can be structured at the deep subwavelength scale and enable routing and guiding of the power flow at a small scale [65–68].

In this paper, we demonstrate a time-reversal invariant acoustic topological insulator [4] in a two-dimensional resonant metamaterial, putting forward the concept of topological acoustic polaritons. We establish the unique relevance of resonant metamaterials as the perfect platform to induce topologically nontrivial acoustic states and force them to undergo predefined pathways, thereby extending the domain of application of topological acoustics to the subwavelength regime.

2. Methods

To create topological acoustic polaritons, we first need to consider a simple physical platform that actually supports polaritonic propagation for sound, before working on inducing a nontrivial topology. Polaritons are hybrid subwavelength states resulting from the interaction between an ensemble of resonators and a propagating wave [69]. When the resonators are assembled on a surface, such states lead to spoof surface polaritons that remain confined to the array. In acoustics, these polaritons are known as spoof surface acoustic waves [70]. As a starting point, we therefore consider a simple two-dimensional array of acoustic resonators, composed of opened empty soda cans arranged in a triangular lattice (figure 1(a)). The cans have a radius of 2.5 cm, a height of 13 cm, and a neck size of about one cm (see supplementary information is available at stacks.iop.org/NJP/19/075003/mmedia for a detailed geometry). The triangular lattice spacing is 6.6 cm. Standard soda cans make very good Helmholtz resonators as their neck has a large cross-sectional area, but is very short, enabling quality factors governed by radiative losses, of the order of 14, and a subwavelength size about $\lambda/12$ at resonance (here 450 Hz) [66]. In panel (b), we plot the acoustic band structure of the crystal in (a), obtained from three-dimensional finite-elements simulations using Comsol Multiphysics. With a single resonator per unit cell (dashed blue box), such a metamaterial naturally supports a single band. As discussed in previous works [66, 67],

this band falls below the sound cone (dashed black lines), i.e. corresponds to subwavelength acoustic states that are localized to the surface: spoof acoustic surface polaritons.

The triangular lattice is a good starting point, as it supports polaritons. However, this polariton does not feature Dirac dispersion at K1 and K1′ points, a key ingredient in the design of topological insulators [5]. To obtain Dirac cones outside of the sound cone, we consider in panel (c) a honeycomb lattice, keeping the same distance between nearest neighbors as in the triangular array of panel (a). The primitive cell of the honeycomb lattice contains two degrees of freedom (green box), leading to two polaritonic bands. The honeycomb lattice can be viewed as the union of two triangular lattices, offset with respect to each other in the ΓM2 direction. The K2/K2′ directions are the only directions in which these sub-lattices form equidistant Bragg planes, leading to a perfect folding of the triangular polaritonic dispersion, which creates the expected degeneracy at K2 and K2′. Note that the second band falls within the sound cone near Γ, but still remains well localized to the surface, with a slow leakage rate to the surrounding space. The slow leakage rate can be understood by the fact that these states possess a strong component in the second Brillouin zone, since they result from band folding. Therefore, all the bands correspond to dark modes that share the principal characteristic of spoof surface polaritons: localization to the surface and deeply subwavelength features [69].

Having obtained Dirac degeneracy, we can start tailoring the topological properties of the crystalline metamaterial. We begin with the observation that in two-dimensional time-reversal invariant topological insulators, one typically starts with two Dirac cones on top of each other, corresponding to time-reversed degenerate partners [4]. Then, nontrivial topology relies on the band crossing of the two degenerate bands, with the topological gap re-opened by an effective gauge potential, a phenomenon associated with band inversion. In our honeycomb lattice however, the two time-reversed Dirac states are located at K2 and K2′. This issue can be solved by considering the extended cell depicted in the red box, which mathematically folds the K2/K2′ points into Γ. In this point of view, the honeycomb lattice is described as a triangular array of hexagons that paves the 2D surface. More importantly, the two Dirac cones are now superposed, and we can now focus on opening a topological band gap.

At this point, the supercell description is merely a mathematical trick. To make it physical, we must modify our crystal to make the extended cell the new primitive cell. To do so, we take inspiration from a method previously proposed by Wu and Hu in the context of non-resonant photonic crystals [31], which consists in changing the size of the hexagon in the extended cell vision, and consider C_6-symmetric triangular lattices of expanded or shrunk hexagons. The method is based on the fact that there exist two 2D irreducible representations of the C_6-symmetry point group at the Γ point corresponding to even and odd parities with respect to the spatial inversion operator. Together with time-reversal symmetry, this property guarantees that the eigenstates at the Γ point always feature a monopolar (s-type) mode, two degenerate dipolar (p-type) modes, two degenerate quadrupolar (d-type) modes, and a hexapolar (f-type) mode. The degeneracy of the dipolar (p_1, p_2) and quadrupolar (d_1, d_2) modes at the Γ point is exploited to build the pseudo-spin states $p_\pm = (p_1 \pm \mathrm{i}p_2)/\sqrt{2}$ and $d_\pm = (d_1 \pm \mathrm{i}d_2)/\sqrt{2}$, with spin-degeneracy being protected by a pseudo time-reversal operator $\mathcal{T} = \mathcal{U}\mathcal{K}$, where $\mathcal{K}$ is the complex conjugation, and $\mathcal{U}$ a rotation operator linked to C_6^v symmetry, with $\mathcal{U}^2 = -1$. The property $T^2 = -1$ guarantees spin degeneracy in C_6^v symmetry, time-reversal invariant systems. Remarkably, we show in the following that the method is also valid to open topological band gaps at the subwavelength scale, and induce nontrivial topological properties for acoustic polaritons supported by resonant metamaterials.

3. Results

3.1. Topological phase transition

As a first possibility for band gap opening, we study the case of the triangular lattice of shrunk hexagons, shown in the inset of figure 2(a) (see supplementary information for the exact description of the geometry). The physical folding of the band structure now results in a complete band gap, and the system is now an insulator near the frequency at which quadruple Dirac degeneracy occurs for the undeformed system, the band structure of which is reproduced in panel (b). A total of six bands is observed, consistent with the number of resonators in the unit cell. Similar to the case of non-resonant crystals [31], the lowest frequency band corresponds to a monopolar s-type mode, with all the resonators within a unit cell excited mostly in phase. The next two bands, shown in red in panels (a), (b), correspond to a dipolar p-type mode, and the next two, in blue, to d-type modes. These four modes, represented in the blue and red boxes, are the modes of interest here, since separated by the insulating band gap. The highest frequency band correspond to a f-type mode, for which adjacent resonators are always out of phase. A very simple picture of the physics occurring in this system consists in considering that the first polariton in the band structure (s-type band) creates a band gap for the other modes of the unit cell, which can now be seen as p-type and d-type resonant defects in this band gap. This way, our acoustic system may

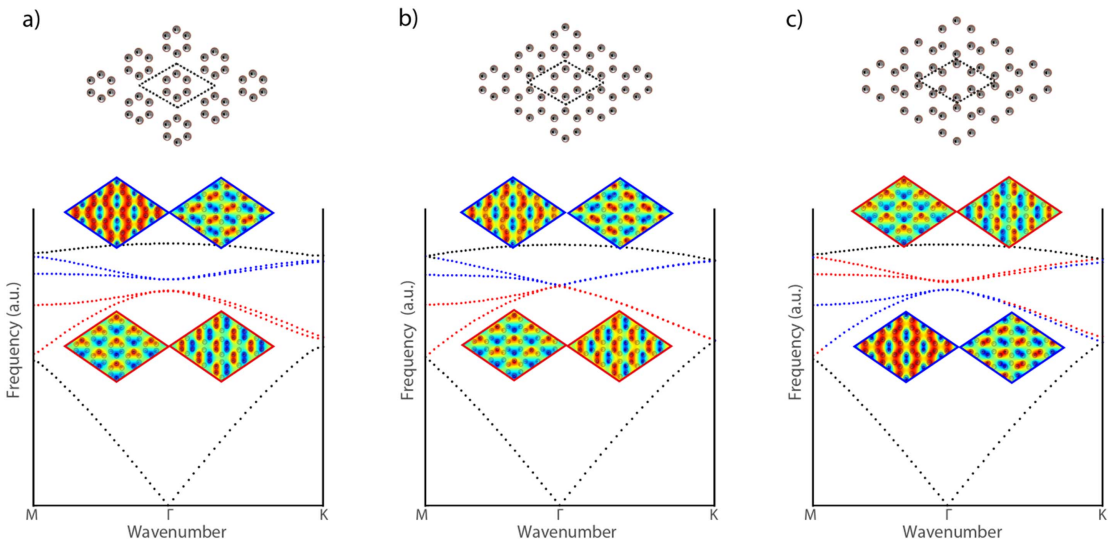

Figure 2. Evolution of the band structure of a deformed honeycomb lattice of Helmholtz resonators, starting from the case of a triangular lattice of small hexagons (panel (a)), and increasing the size of the hexagons (panels (b) and (c)). The red bands correspond to p-type polaritons, whereas the red bands are associated with d-type polaritons. The trivial insulator in (a) undergoes a topological transition, as the gap closes in (b) and reopens with an inverted band structure in (c).

adequately be described by the tight binding model presented in [32], which considers the topological properties of electrons in a honeycomb lattice with detuned hopping energies. An important point is that the two p-type and d-type bands remain degenerate at the Γ point, consistent with the two two-dimensional representations of the C_6 point group [71]. Following the usual method [31, 32, 54], this degeneracy is exploited to define a pseudospin pair in these bands, and a pseudo time-reversal operator related to C_6 symmetry, that protects the presence of Kramers partners at Γ.

As we increase the size of the hexagons, we reach the point where the lattice becomes the initial pure honeycomb lattice (panel (b)), and the gap closes, consistent with the band folding process described in methods. As we further increase the size of the hexagons, the gap reopens, however the position of the p and d bands is now inverted near Γ. Such a band inversion, symptomatic of the topological transition that occurs as the gap reopens, is characterized by a nonzero $\mathbb{Z}_2$ topological invariant [32]. To verify this, we have numerically computed the spin-Chern numbers of the bands using the method by Fukui, Hatsugai and Suzuki [72], which allows for the determination of the topological invariants on a discretized portion of the Brillouin zone around the Γ point. As expected, we found zero spin-Chern numbers in the case of the shrunk hexagon lattice. Differently, the expanded hexagon lattice has spin-Chern numbers equal to ± 1 for the $p_\pm$ bands and ∓ 1 for $d_\pm$. This is a direct confirmation of the nontrivial topology of the bands. As we go away from the Γ point, the pseudo-time reversal symmetry is gradually broken, and the two pseudo-spin channels start to couple to each other. For sufficiently small gap openings, this has no effect on the topology, which is determined in a small region around Γ.

3.2. Edge states

A remarkable property of topological insulators is the appearance of chiral edge states at the boundary between domains with different topological properties [9]. To study these edge modes, we design two different arrays of acoustic Helmholtz resonators, one with trivial topology (following figure 2(a)), and one with nontrivial topology (as in figure 2(c)). The bulk band structures of these two crystals, respectively plotted in figure 3(a) in red and blue, are designed to support band gaps of identical sizes. Next, we form a supercell with a boundary along ΓK3 (see supplementary information for the detailed geometry), and solve for the dispersion of interface modes travelling in that direction, applying periodic boundary conditions. We obtain four band gap crossing edge modes, corresponding to two time-reversed pairs per interface, represented by red lines in figure 3(b). In figure 3(c), we represent the acoustic intensity of one of the edge modes. The interface (dashed line) is located at the center of panel (c), along the horizontal direction. We also represent in red the intensity profile in the transverse direction. This allows us to calculate the in-plane decay distance, corresponding to the distance after which the exponential envelope of the intensity has decayed by a factor $1/e = 0.37$. We obtain a decay length of 0.46λ, confirming the in-plane subwavelength localization of the modes at the domain wall.

Remark that, since the hexagons on each side of the interface do not have the same size, such a boundary effectively breaks C_6 symmetry, therefore lifting spin degeneracy, similar to quantum spin Hall systems in the

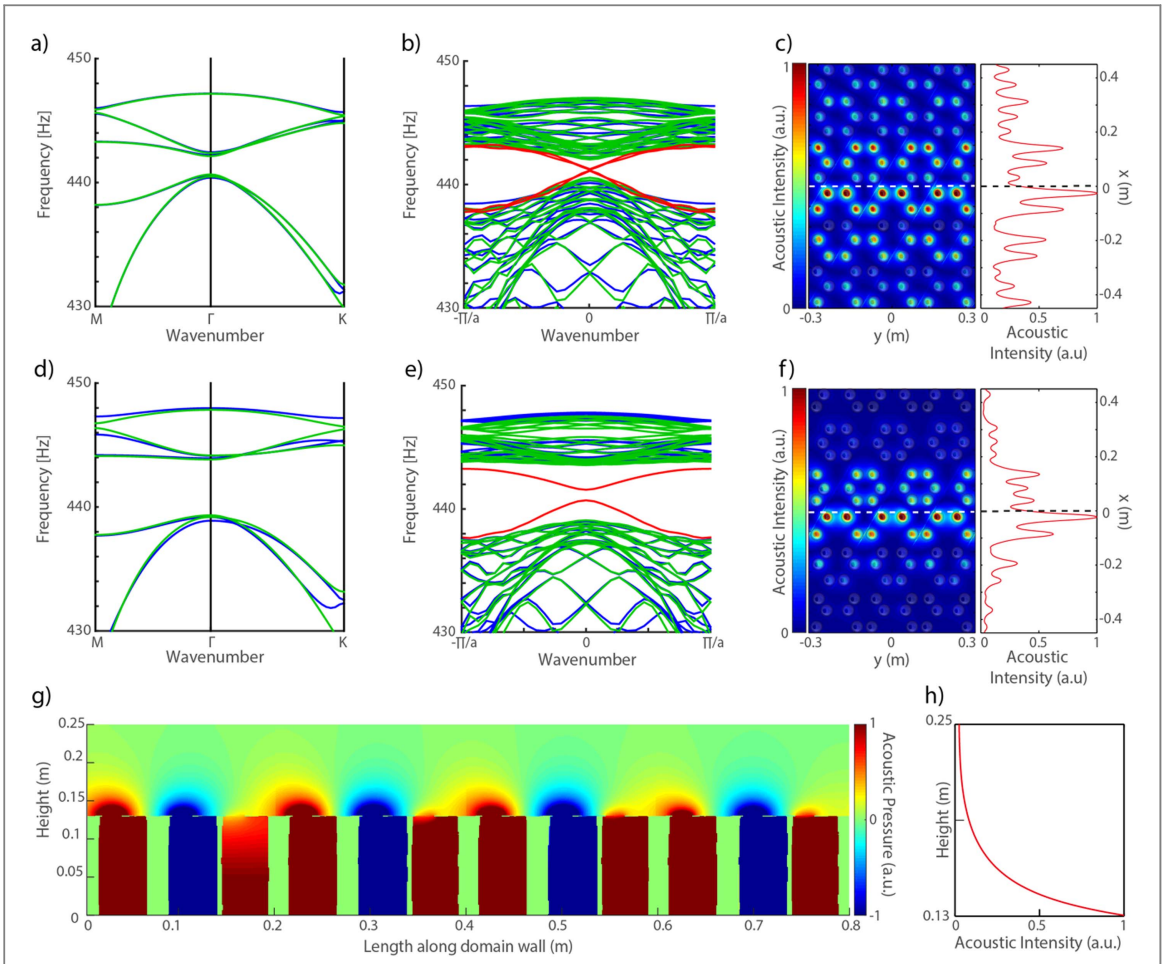

Figure 3. Topological acoustic spoof surface polaritons localized at interfaces between a topologically trivial and a topologically nontrivial domain. Panel (a): bulk band structure of the topologically trivial domain (blue) and the topologically nontrivial domain (green). Panel (b): Acoustic band structure for a 1 by 20 supercell with a domain wall at the center (edge modes shown in red). Panel (c): Intensity profile for an acoustic polariton localized to the interface. The red curve represents the intensity in the transverse direction. Panels (d)–(f): Same as (a), (b), (c) but for larger gap sizes. Panel (g): Acoustic pressure distribution along the interface for the edge state, illustrating the subwavelength confinement in the out-of-plane direction. Panel (h): evolution of the acoustic intensity of the edge mode in the vertical (out-of-plane) direction.

presence of magnetic defects. As a result, the edge states are gapped, and do not completely cross the gap from one bulk band to the other. In panels (a)–(c), however, this effect is nearly invisible, due to the very small difference between the hexagons in the trivial and topological domains, leading to a very weak breaking of C_6 symmetry. To highlight this further, we consider in panels (d)–(f) the case of a larger bandgap, generated by deforming further the hexagons on both sides of the interface. We see that larger band gaps (panel (d)) lead to gapped edge states (panel (e)) that are more confined to the interface (panel (f)), in-plane decay distance of 0.25λ). In panel (g), we represent the acoustic pressure for the edge mode along the interface, underlining the strong subwavelength confinement of the acoustic state also in the out-of-plane direction. Panel (h) illustrates this further by representing the exponential decay of the acoustic intensity in the vertical direction. Remarkably, topological surface acoustic polaritons are localized in subwavelength volumes in both the in-plane and out-of-plane directions. Note that these edge modes are *topological*, since they owe their existence to the difference in the topology of the two surrounding bulks, however they are not strictly speaking *topologically protected*, as C_6 symmetry is broken at the interface. This is not necessarily a problem in practice since one can design adiabatic interfaces, slowly deforming one medium into one another, so that the crystal remains locally C_6 symmetric.

Figure 4 studies the effect of different gap sizes for the topological and trivial domains. In panels (a)–(c), we repeat our study by assuming that the band gap of the band structure of the trivial insulator (blue bands) is much larger than the gap of the topological band structure (green bands). Panels (d)–(f) consider the opposite situation. In both cases, we observe that edge modes (in red) always exist in the frequency band corresponding to the intersection of the two gaps. The mode profiles (c) and (g) demonstrate that the edge mode extends further in the domain where the gap is the smallest, consistent with the fact that the imaginary part of the Bloch wave number in the transverse direction usually increases with the gap size. In panel (c), the decay length in the topological and trivial samples are 0.47λ and 0.23λ, respectively. In panel (d), they are 0.2λ and 0.47λ,

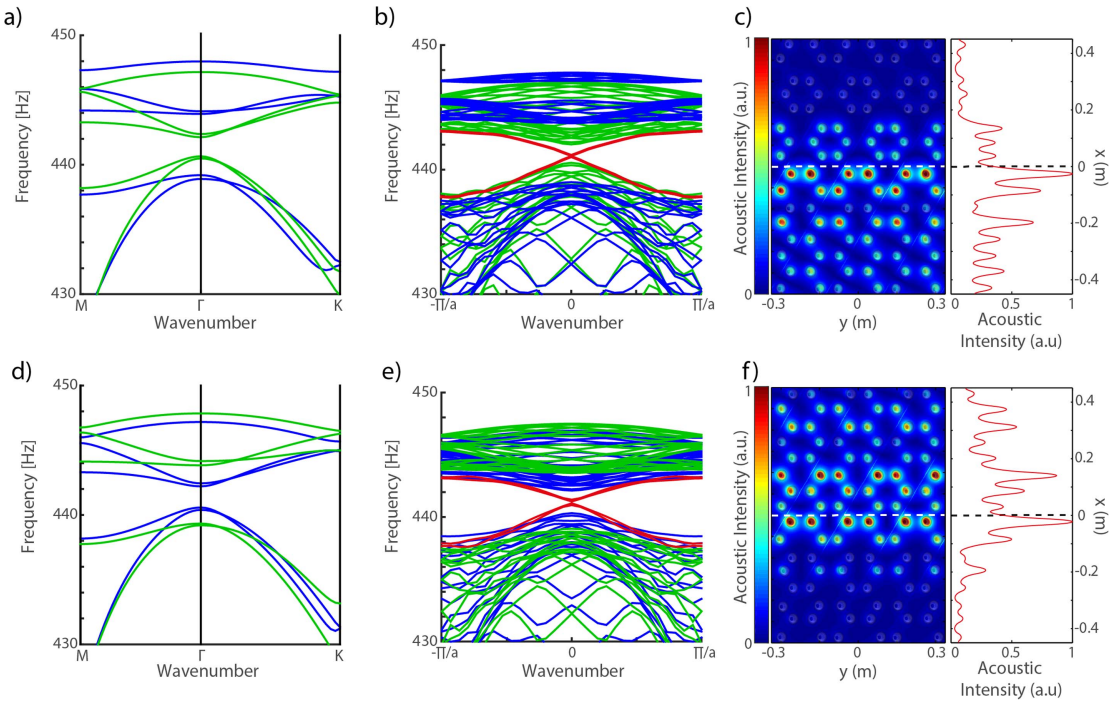

Figure 4. Same as figure 3, but for band gaps of dissimilar sizes. Panels (a)–(c): The trivial gap is larger than the topological gap. Panels (d)–(f): The topological gap is larger than the trivial gap.

respectively. In all cases, the confinement along the vertical direction is associated with a decay length of 0.03λ. Therefore, the topological polaritons are confined to subwavelength distances both in the plane of the array and in the normal direction. We conclude that an asymmetry in the size of the band gap does not alter the presence of edge states, and allows for full control of their in-plane localization with respect to the interface.

3.3. Robust guiding of sound along subwavelength channels

Since it is not possible to construct a one-dimensional interface without breaking C_6 symmetry, we cannot completely avoid coupling between the two spin degrees of freedom at a boundary. For topological insulators based on C_6 symmetry, despite the fact that the bulk crystal is topological, the rest of the world is necessarily magnetic, and the topological edge states are not topologically protected. The natural question that arises is: are the acoustic edge modes still robust enough to have practical interest? To address this question, we perform the numerical experiment presented in figure 5(a). We consider a finite-size crystal with two domains with distinct topology. The top domain (green box), belongs to the topological crystal phase, whereas the bottom domain (blue box) has a trivial topology. The boundary between the two, highlighted in red, features a total of six sharp turns with radii of curvature much smaller than the wavelength. We place a source of acoustic waves on the left side, right on the boundary. On the left-hand side of the source, and after the last turn, we adiabatically increase the level of absorption losses in order to create a crystalline version of perfectly matched layers (PML), and guarantee no reflections at the edge of the interface. The frequency of the source is tuned in order to excite the edge mode near Γ. The band gaps for both domains are of equal sizes, and we consider two different scenarios. In the first one (panel (b)), the band gap is small, as in figure 3(a), whereas in panel (c) the band gap is larger, as in figure 3(d). Remarkably, we see in panel (b) that the edge mode is capable of traveling along the irregularly shaped interface despite the presence of stringent detours involving sharp turns. Normally, any conventional acoustic waveguide undergoing turns with subwavelength radii of curvature would be subject to large Fabry-Pérot interferences due to multiple reflections at the turns. Extraordinarily here, the intensity of the surface acoustic polariton is constant along the edge, demonstrating the absence of backscattering and the inherently robust transport of the acoustic power. In panel (c), the difference between the hexagons on both sides of the interface is more pronounced, leading to a larger breaking of C_6 symmetry by the interface. As a consequence, the edge mode should be less robust. This is indeed observed in the panel, as the intensity value slightly fluctuates along the interface. This effect, however, remains relatively weak, and a significant portion of the acoustic power is transmitted to the PML, even after six severe turns. We conclude that the breaking of C_6 symmetry is not a fundamental issue in practice, and even though the topological edge mode is not, strictly speaking, topologically protected, it is still extremely robust. This robustness is the strongest at the Γ point, consistent with the fact that

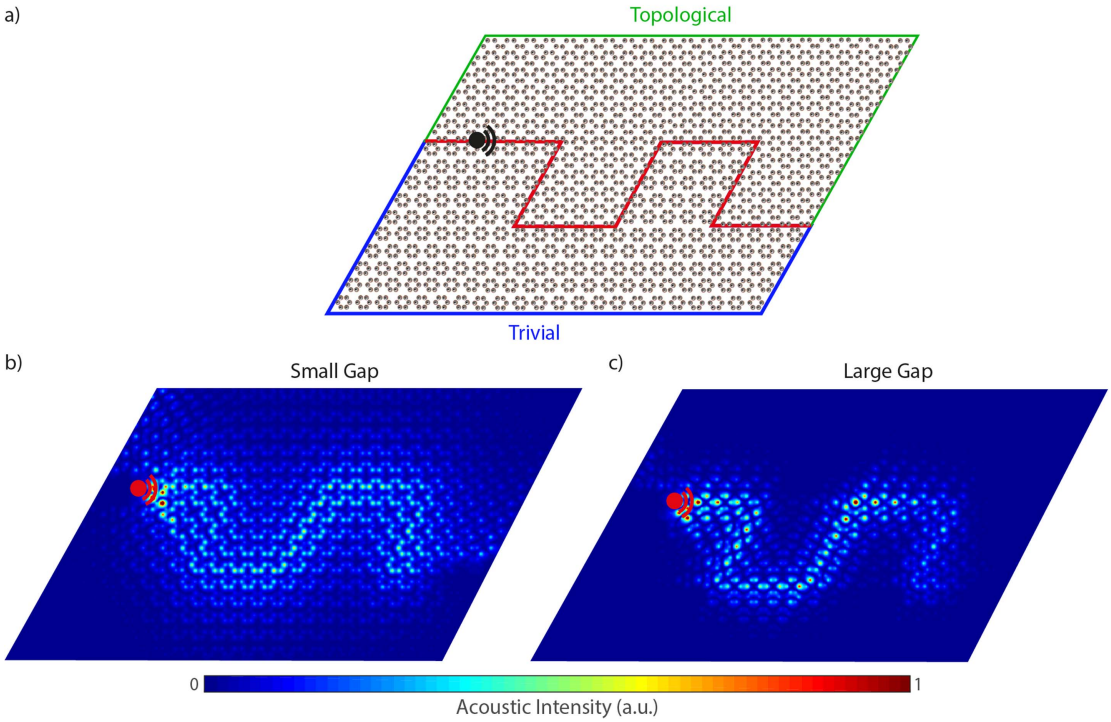

Figure 5. Demonstration of robust backscattering-immune guiding of spoof surface acoustic polaritons along arbitrary pathways with subwavelength features. Panel (a): We create a finite-size sample containing topological (green box) and trivial (blue box) crystal domains, and place a source at the interface (red boundary). Perfectly matched layers are inserted near the source on the left and at the end of the domain wall. Panel (b): Resulting acoustic intensity in the case of the small gap of figure 3(a). Panel (b): Resulting acoustic intensity in the case of the larger gap of figure 3(d).

spin degeneracy is progressively lifted as we go away from the Brillouin zone center [32]. We have also observed topological edge modes between the topological crystal and the air, however these modes are not very robust due to the larger breaking of six-fold rotational symmetry at such an interface.

4. Discussion and conclusion

We have put forward and demonstrated the concept of topological spoof surface acoustic polaritons, enabling robust backscattering-immune guiding of sound on a metasurface, along subwavelength paths with arbitrary shapes. The design, based on a two-dimensional array of subwavelength acoustic Helmholtz resonators with a tailored internal structure, supports acoustic chiral edge polaritons propagating at the interface between domains of distinct topology. We stress that the physical platform presented here is just one among the many different solutions to implement topological polaritons, and the concept can easily be transposed to elastic, mechanical or electromagnetic waves. In audible acoustics, other types of resonators can be envisioned to mitigate the impact of viscoelastic losses on wave propagation. We have highlighted a tradeoff between bandwidth, localization and robustness, demonstrating unusual resilience of the subwavelength edge modes to stringent detours and turns even for the most localized states. Compared with previous designs based on C_6 symmetry and non-resonant structures [31, 54], our proposal operates in the deep subwavelength regime (typical in-plane decay length of 0.25λ, out-of-plane decay length of 0.03λ) and directly on a surface, avoiding the use of a bulky crystal and massive waveguides. In addition, our system is opened to its environment, and by operating within the sound cone, topological acoustic states can be coupled to the radiation continuum. This opens interesting application perspectives for topological acoustic polaritons, which may enable disruptive advances in transducer or sensing technologies, including a new generation of topologically protected acoustic leaky wave antennas [73–76] and subwavelength imaging systems [67]. In addition, the slow group velocity of topological acoustic polaritons may be of significant interest to realize robust slow wave systems, avoiding their typical sensitivity to disorder. Extended to the subwavelength regime, topological acoustic phases may lead to unique advances in our ability to control and guide phonons with extremely compact devices and an inherent robustness to fabrication defects. Our proposal opens new possibilities in wave engineering by extending the concept of topological insulators down to the subwavelength scale.

Acknowledgments

R Fleury would like to thank the support of the Acoustical Society of America through the Frederick V Hunt Postdoctoral Research Fellowship in Acoustics. The research leading to these results has received funding from the People Program (Marie Curie Actions) of the European Union's Seventh Framework Program (FP7/2007–2013) under REA grant agreement n. PCOFUND-GA-2013-609102, through the PRESTIGE program coordinated by Campus France.

Authors contribution statement

SY and RF developed the concept and performed the numerical simulations. SY made the figures. RF wrote the paper. FL, MF, and GL supervised the project. All authors contributed to the elaboration of the manuscript.

References

[1] Klitzing K V, Dorda G and Pepper M 1980 New method for high-accuracy determination of the fine-structure constant based on quantized Hall resistance *Phys. Rev. Lett.* **45** 494–7
[2] Thouless D J, Kohmoto M, Nightingale M P and den Nijs M 1982 Quantized Hall conductance in a two-dimensional periodic potential *Phys. Rev. Lett.* **49** 405–8
[3] Simon B 1983 Holonomy, the quantum adiabatic theorem, and Berry's phase *Phys. Rev. Lett.* **51** 2167–70
[4] Kane C L and Mele E J 2005 Z_2 topological order and the quantum spin Hall effect *Phys. Rev. Lett.* **95** 146802
[5] Kane C L and Mele E J 2005 Quantum spin Hall effect in graphene *Phys. Rev. Lett.* **95** 226801
[6] Bernevig B A, Hughes T L and Zhang S-C 2006 Quantum spin Hall effect and topological phase transition in HgTe quantum wells *Science* **314** 1757–61
[7] Hsieh D, Qian D, Wray L, Xia Y, Hor Y S, Cava R J and Hasan M Z 2008 A topological Dirac insulator in a quantum spin Hall phase *Nature* **452** 970–4
[8] Zhang H, Liu C-X, Qi X-L, Dai X, Fang Z and Zhang S-C 2009 Topological insulators in Bi_2Se_3, Bi_2Te_3 and Sb_2Te_3 with a single Dirac cone on the surface *Nat. Phys.* **5** 438–42
[9] Hasan M Z and Kane C L 2010 Colloquium: topological insulators *Rev. Mod. Phys.* **82** 3045–67
[10] Qi X-L and Zhang S-C 2011 Topological insulators and superconductors *Rev. Mod. Phys.* **83** 1057–110
[11] Raghu S and Haldane F 2008 Analogs of quantum-Hall-effect edge states in photonic crystals *Phys. Rev.* A **78** 33834
[12] Haldane F and Raghu S 2008 Possible realization of directional optical waveguides in photonic crystals with broken time-reversal symmetry *Phys. Rev. Lett.* **100** 13904
[13] Wang Z, Chong Y D, Joannopoulos J D and Soljačić M 2008 Reflection-free one-way edge modes in a gyromagnetic photonic crystal *Phys. Rev. Lett.* **100** 13905
[14] Wang Z, Chong Y, Joannopoulos J D and Soljacić M 2009 Observation of unidirectional backscattering-immune topological electromagnetic states *Nature* **461** 772–5
[15] Hafezi M, Demler E A, Lukin M D and Taylor J M 2011 Robust optical delay lines with topological protection *Nat. Phys.* **7** 907–12
[16] Fang K, Yu Z and Fan S 2012 Realizing effective magnetic field for photons by controlling the phase of dynamic modulation *Nat. Photon.* **6** 782–7
[17] Khanikaev A B, Mousavi S H, Tse W-K, Kargarian M, MacDonald A H and Shvets G 2013 Photonic topological insulators *Nat. Mater.* **12** 233–9
[18] Hafezi M, Mittal S, Fan J, Migdall A and Taylor J M 2013 Imaging topological edge states in silicon photonics *Nat. Photon.* **7** 1001–5
[19] Lu L, Fu L, Joannopoulos J D and Soljačić M 2013 Weyl points and line nodes in gyroid photonic crystals *Nat. Photon.* **7** 294–9
[20] Rechtsman M C, Zeuner J M, Plotnik Y, Lumer Y, Podolsky D, Dreisow F, Nolte S, Segev M and Szameit A 2013 Photonic Floquet topological insulators *Nature* **496** 196–200
[21] Liang G Q and Chong Y D 2013 Optical resonator analog of a two-dimensional topological insulator *Phys. Rev. Lett.* **110** 203904
[22] Mittal S, Fan J, Faez S, Migdall A, Taylor J M and Hafezi M 2014 Topologically robust transport of photons in a synthetic gauge field *Phys. Rev. Lett.* **113** 87403
[23] Pasek M and Chong Y D 2014 Network models of photonic Floquet topological insulators *Phys. Rev.* B **89** 75113
[24] Chen W-J, Jiang S-J, Chen X-D, Zhu B, Zhou L, Dong J-W and Chan C T 2014 Experimental realization of photonic topological insulator in a uniaxial metacrystal waveguide *Nat. Commun.* **5** 5782
[25] Skirlo S A, Lu L and Soljačić M 2014 Multimode one-way waveguides of large Chern numbers *Phys. Rev. Lett.* **113** 113904
[26] Skirlo S A, Lu L, Igarashi Y, Yan Q, Joannopoulos J and Soljačić M 2015 Experimental observation of large Chern numbers in photonic crystals *Phys. Rev. Lett.* **115** 253901
[27] Ningyuan J, Owens C, Sommer A, Schuster D and Simon J 2015 Time- and site-resolved dynamics in a topological circuit *Phys. Rev.* X **5** 21031
[28] Gao W, Lawrence M, Yang B, Liu F, Fang F, Béri B, Li J and Zhang S 2015 Topological photonic phase in chiral hyperbolic metamaterials *Phys. Rev. Lett.* **114** 37402
[29] Ma T, Khanikaev A B, Mousavi S H and Shvets G 2015 Guiding electromagnetic waves around sharp corners: topologically protected photonic transport in metawaveguides *Phys. Rev. Lett.* **114** 127401
[30] Hu W, Pillay J C, Wu K, Pasek M, Shum P P and Chong Y D 2015 Measurement of a topological edge invariant in a microwave network *Phys. Rev.* X **5** 11012
[31] Wu L-H and Hu X 2015 Scheme for achieving a topological photonic crystal by using dielectric material *Phys. Rev. Lett.* **114** 223901
[32] Wu L-H and Hu X 2016 Topological properties of electrons in honeycomb lattice with detuned hopping energy *Sci. Rep.* **6** 24347
[33] Lu L, Wang Z, Ye D, Ran L, Fu L, Joannopoulos J D and Soljačić M 2015 Experimental observation of Weyl points *Science* **349** 622–4
[34] Silveirinha M G 2016 Z 2 topological index for continuous photonic materials *Phys. Rev.* B **93** 75110
[35] Cheng X, Jouvaud C, Ni X, Mousavi S H, Genack A Z and Khanikaev A B 2016 Robust reconfigurable electromagnetic pathways within a photonic topological insulator *Nat. Mater.* **15** 542–8
[36] Gao F *et al* 2016 Probing topological protection using a designer surface plasmon structure *Nat. Commun.* **7** 11619
[37] Lu L, Fang C, Fu L, Johnson S G, Joannopoulos J D and Soljačić M 2016 Symmetry-protected topological photonic crystal in three dimensions *Nat. Phys.* **12** 337–40

[38] Prodan E and Prodan C 2009 Topological phonon modes and their role in dynamic instability of microtubules *Phys. Rev. Lett.* **103** 248101
[39] Kane C L and Lubensky T C 2013 Topological boundary modes in isostatic lattices *Nat. Phys.* **10** 39–45
[40] Chen B G, Upadhyaya N and Vitelli V 2014 Nonlinear conduction via solitons in a topological mechanical insulator *Proc. Natl Acad. Sci. USA* **111** 13004–9
[41] Paulose J, Chen B G and Vitelli V 2015 Topological modes bound to dislocations in mechanical metamaterials *Nat. Phys.* **11** 153–6
[42] Paulose J, Meeussen A S and Vitelli V 2015 Selective buckling via states of self-stress in topological metamaterials *Proc. Natl Acad. Sci. USA* **112** 7639–44
[43] Nash L M, Kleckner D, Read A, Vitelli V, Turner A M and Irvine W T M 2015 Topological mechanics of gyroscopic metamaterials *Proc. Natl Acad. Sci. USA* **112** 14495–500
[44] Wang P, Lu L and Bertoldi K 2015 Topological phononic crystals with one-way elastic edge waves *Phys. Rev. Lett.* **115** 104302
[45] Susstrunk R and Huber S D 2015 Observation of phononic helical edge states in a mechanical topological insulator *Science* **349** 47–50
[46] Rocklin D Z, Chen B G, Falk M, Vitelli V and Lubensky T C 2016 Mechanical Weyl modes in topological Maxwell lattices *Phys. Rev. Lett.* **116** 135503
[47] Khanikaev A B, Fleury R, Mousavi S H and Alù A 2015 Topologically robust sound propagation in an angular-momentum-biased graphene-like resonator lattice *Nat. Commun.* **6** 8260
[48] Yang Z, Gao F, Shi X, Lin X, Gao Z, Chong Y and Zhang B 2015 Topological acoustics *Phys. Rev. Lett.* **114** 114301
[49] Mousavi S H, Khanikaev A B and Wang Z 2015 Topologically protected elastic waves in phononic metamaterials *Nat. Commun.* **6** 8682
[50] Ni X, He C, Sun X-C, Liu X, Lu M-H, Feng L and Chen Y-F 2015 Topologically protected one-way edge mode in networks of acoustic resonators with circulating air flow *New J. Phys.* **17** 53016
[51] Fleury R, Khanikaev A B and Alù A 2016 Floquet topological insulators for sound *Nat. Commun.* **7** 11744
[52] Xiao M, Chen W-J, He W-Y and Chan C T 2015 Synthetic gauge flux and Weyl points in acoustic systems *Nat. Phys.* **11** 920–4
[53] Peano V, Brendel C, Schmidt M and Marquardt F 2015 Topological phases of sound and light *Phys. Rev.* X **5** 31011
[54] He C, Ni X, Ge H, Sun X-C, Chen Y-B, Lu M-H, Liu X-P and Chen Y-F 2016 Acoustic topological insulator and robust one-way sound transport *Nat. Phys.* **12** 1124–9
[55] Salerno G, Ozawa T, Price H M and Carusotto I 2016 Floquet topological system based on frequency-modulated classical coupled harmonic oscillators *Phys. Rev.* B **93** 85105
[56] Pal R K, Schaeffer M and Ruzzene M 2016 Helical edge states and topological phase transitions in phononic systems using bi-layered lattices *J. Appl. Phys.* **119** 84305
[57] Vishwanath A and Senthil T 2013 Physics of three-dimensional bosonic topological insulators: surface-deconfined criticality and quantized magnetoelectric effect *Phys. Rev.* X **3** 11016
[58] Ye P and Gu Z-C 2015 Vortex-line condensation in three dimensions: a physical mechanism for bosonic topological insulators *Phys. Rev.* X **5** 21029
[59] Casimir H B G 1945 On Onsager's principle of microscopic reversibility *Rev. Mod. Phys.* **17** 343–50
[60] Jalas D *et al* 2013 What is—and what is not—an optical isolator *Nat. Photon.* **7** 579–82
[61] Maznev A A, Every A G and Wright O B 2013 Reciprocity in reflection and transmission: what is a 'phonon diode'? *Wave Motion* **50** 776–84
[62] Fleury R, Sounas D L, Sieck C F, Haberman M R and Alù A 2014 Sound isolation and giant linear nonreciprocity in a compact acoustic circulator *Science* **343** 516–9
[63] Fleury R, Sounas D L, Haberman M R and Alù A 2015 Nonreciprocal acoustics *Acoust. Today* **11** 14
[64] Fleury R, Sounas D L and Alù A 2015 Subwavelength ultrasonic circulator based on spatiotemporal modulation *Phys. Rev.* B **91** 174306
[65] Lemoult F, Fink M and Lerosey G 2011 Acoustic resonators for far-field control of sound on a subwavelength scale *Phys. Rev. Lett.* **107** 64301
[66] Lemoult F, Kaina N, Fink M and Lerosey G 2012 Wave propagation control at the deep subwavelength scale in metamaterials *Nat. Phys.* **9** 55–60
[67] Kaina N, Lemoult F, Fink M and Lerosey G 2015 Negative refractive index and acoustic superlens from multiple scattering in single negative metamaterials *Nature* **525** 77–81
[68] Lemoult F, Kaina N, Fink M and Lerosey G 2016 Soda cans metamaterial: a subwavelength-scaled phononic crystal *Crystals* **6** 82
[69] Pendry J B, Martín-Moreno L and Garcia-Vidal F J 2004 Mimicking surface plasmons with structured surfaces *Science* **305** 847–8
[70] Jia H, Lu M, Wang Q, Bao M and Li X 2013 Subwavelength imaging through spoof surface acoustic waves on a two-dimensional structured rigid surface *Appl. Phys. Lett.* **103** 103505
[71] Bradley C J and Cracknell A P 1972 *The Mathematical Theory of Symmetry in Solids* (Oxford: Clarendon)
[72] Fukui T, Hatsugai Y and Suzuki H 2005 Chern numbers in discretized brillouin zone: efficient method of computing (spin) Hall conductances *J. Phys. Soc. Japan* **74** 1674–7
[73] Naify C J, Guild M D, Rohde C A, Calvo D C and Orris G J 2015 Demonstration of a directional sonic prism in two dimensions using an air-acoustic leaky wave antenna *Appl. Phys. Lett.* **107** 133505
[74] Naify C J, Rogers J S, Guild M D, Rohde C A and Orris G J 2016 Evaluation of the resolution of a metamaterial acoustic leaky wave antenna *J. Acoust. Soc. Am.* **139** 3251–8
[75] Esfahlani H, Karkar S, Lissek H and Mosig J R 2016 Exploiting the leaky-wave properties of transmission-line metamaterials for single-microphone direction finding *J. Acoust. Soc. Am.* **139** 3259–66
[76] Esfahlani H, Karkar S, Lissek H and Mosig J R 2016 Acoustic dispersive prism *Sci. Rep.* **6** 18911